JOURNAL OF GUIDANCE, CONTROL, AND DYNAMICS
Vol. 32, No. 5, September–October 2009

Investigation into Crossover Regression in Compensatory Manual Tracking Tasks

G. C. Beerens,* H. J. Damveld,† M. Mulder,‡ M. M. van Paassen,§ and J. C. van der Vaart¶
Delft University of Technology, 2600 GB Delft, The Netherlands

DOI: 10.2514/1.43528

This paper investigates the crossover-regression phenomenon in compensatory manual-control tasks. The adjustment, between-subject variation, and accuracy of linear human-operator models are analyzed in detail. A theoretical investigation into closed-loop error minimization will be presented. Our main hypothesis was that crossover regression is caused by an operator's inability to sufficiently decrease the time delays required to limit forcing-function resonance. To test the hypothesis and explore the use of linear-operator models in regressed conditions, an experiment very similar to McRuer's landmark 1965 experiment was conducted. A comparison between regressive and nonregressive conditions revealed that crossover regression is indeed a strategy to reduce forcing-function resonance. The bandwidth of the forcing-function signal at which participants regressed their crossover frequency was found to vary considerably between participants. In regressed conditions, the between-subject variability in frequency-domain performance increased. Additionally, the operator control behavior became increasingly nonlinear, resulting in larger uncertainties and a higher between-subject variability in the linear-model parameter estimates.

Nomenclature

$e(t)$	=	tracking error, in.
K_c	=	controlled dynamics gain, in./in.
$n(t)$	=	operator remnant activity, deg
T	=	measurement time, s
$u(t)$	=	stick deflection, deg
$Y_c(j\omega)$	=	controlled element dynamics
$Y_p(j\omega)$	=	pilot describing function
$y(t)$	=	system output, in.
ζ	=	damping ratio
$\rho^2(\omega)$	=	squared correlation coefficient
ρ_a^2	=	squared relative remnant
σ_i	=	forcing-function standard deviation, in.
τ_e	=	effective time delay, s
τ_d	=	pure time delay, s
τ_I	=	lag-time constant, s
τ_L	=	lead-time constant, s
φ_M	=	phase margin, deg
$\varphi(\omega)$	=	phase shift, deg
ω_c	=	gain crossover frequency, rad/s
ω_i	=	forcing-function bandwidth, rad/s
ω_{nm}	=	neuromuscular break frequency, rad/s

Presented as Paper 7112 at the AIAA Modeling and Simulation Technologies Conference and Exhibit, Honolulu, HI, 18–21 August 2008; received 30 January 2009; revision received 21 April 2009; accepted for publication 23 April 2009.

*Research Associate, Control and Simulation Division, Faculty of Aerospace Engineering, Post Office Box 5058; gijsbeerens@gmail.com.

†Research Associate, Control and Simulation Division, Faculty of Aerospace Engineering, Post Office Box 5058; h.j.damveld@tudelft.nl.

‡Professor, Control and Simulation Division, Faculty of Aerospace Engineering, P.O. Box 5058; m.mulder@tudelft.nl. Member AIAA.

§Associate Professor, Control and Simulation Division, Faculty of Aerospace Engineering, Post Office Box 5058; m.m.vanpaassen@tudelft.nl. Member AIAA.

¶Associate Professor, Control and Simulation Division, Faculty of Aerospace Engineering, Post Office Box 5058; j.c.vandervaart@tudelft.nl.

I. Introduction

CROSSOVER regression in manual control is a control strategy where the human operator reduces the tracking bandwidth to improve closed-loop performance [1]. In the literature, many occurrences of crossover regression in manual-control tasks can be found. These are caused by changes in forcing-function bandwidth [1], controlled element dynamics [1–5], degraded display characteristics [6], and divided attention tasks [7].

One generally accepted explanation for crossover regression is given in McRuer et al.'s landmark 1965 report [1]: crossover regression results in smaller mean-squared tracking errors when the forcing-function bandwidth approximates the crossover frequency. This explanation, however, is limited to certain classes of controlled system dynamics and a specific type of forcing function; much remains unexplained. First of all, a general cause of crossover regression in the earlier mentioned cases is unknown. It is also not clear how the human operator adjusts his or her neuromuscular dynamics and equalization selection when regression occurs. Effects of between-subject variability have seldom been reported. Furthermore, it was observed in experiments that the linearity of the control behavior decreased when crossover regression occurred [8,9]. This raises questions whether linear models still apply in regressed conditions, and also whether the corresponding parameter estimation techniques are still valid. The occurrence of crossover regression in previous experiments, both expected [5,6,10] and unexpected [8,9], and our recent work on developing a handling quality assessment method based on crossover regression [3,4], renewed our interest.

The objectives of this paper are twofold: first, more insight needs to be obtained into the phenomenon of crossover regression and the associated adjustment, between-subject variation, and accuracy of linear-operator control-model parameter estimates. Second, to predict more accurately whether crossover regression might occur in experiments, more knowledge regarding the possible causes of crossover regression is desired.

The paper has two parts. First, the main findings of previous studies into crossover regression are summarized. By means of a theoretical analysis, an explanation for the maximum closed-loop input-to-error amplification ratio is derived, relating crossover regression to human-operator time-delay constraints. The second part describes an experiment, designed to replicate the Systems Technology, Inc. (STI) experiment. This experiment was conducted to test our hypotheses and to investigate the changes in operator-model parameters between conditions with and without crossover

regression. The paper concludes with a summary of the main findings observed in the theoretical and experimental analyses.

II. Previous Investigations into Crossover Regression

Crossover-regression has been observed using all basic types of controlled element dynamics (proportional [11], rate [12], and acceleration [1]), as well as aircraft dynamics [3,4]. Elkind was the first to encounter crossover regression in an experiment with proportional controlled element dynamics [11]. He observed that, for the bandpass conditions,** the operator gain decreased when forcing-function bandwidth increased.

Further research into crossover regression for compensatory tracking tasks with a central visual display was reported by McRuer et al. [1]. Their experiment combined proportional, rate, and acceleration controlled system dynamics Y_c with three forcing functions containing bandwidths ω_i of 1.5, 2.5, and 4.0 rad/s. We will refer to this experiment as "the STI experiment" with STI 6-4, 7-3, and 8-2 forcing functions; the numbers denote the number of high-magnitude and low-magnitude sinusoids.

To model the quasi-nonlinear human operator, McRuer et al. [1] studied operator control behavior in the frequency domain. The human operator is decomposed into a linear describing function Y_p and remnant n, which is the part of the response for which the linear part cannot account. This is illustrated in Fig. 1. The linear part should be such that it results in similar responses as the quasi-nonlinear human operator, when excited by the same forcing function i.

McRuer et al.'s [1] crossover model (COM) describes the systematic adaptation of operators to various types of controlled dynamics and forcing functions. Its main assumption is that operators adopt a sufficient lead–lag equalization, such that the open loop approximates integratorlike dynamics in the crossover region, with sufficiently large stability margins:

$$Y_{\text{ol}}(j\omega) = Y_p(j\omega)Y_c(j\omega) \doteq \frac{\omega_c}{j\omega} e^{-j\omega\tau_e^{\text{com}}}; \quad \text{when } \omega \approx \omega_c \qquad (1)$$

The COM is composed of two parameters: the effective time delay τ_e^{com}, and the (gain) crossover frequency ω_c. For performance, the crossover frequency should exceed the forcing-function bandwidth ω_i to warrant an adequate response.

The crossover frequencies measured in the STI experiment are shown in Fig. 2. The crossover frequency ω_{c_0} depends explicitly on the controlled dynamics Y_c and is defined as the value of ω_c when extrapolated to $\omega_i = 0$. The figure shows that, for increasing forcing-function bandwidth, the crossover frequency slightly increases. Regression was only found for the STI 8-2 forcing function with double integrator dynamics [1].

Variations in operator-model parameters, measured in the STI experiment, led to the definition of the verbal adjustment rules [13]. Rule 4c relates the occurrence of crossover regression to the forcing-function bandwidth and the controlled element dynamics: "when ω_i nears or becomes greater than $0.8\omega_{c_0}$, the crossover frequency regresses to values much lower than ω_{c_0}," or

$$\omega_i < 0.8\omega_{c_0} \qquad (2)$$

This inequality, also included in Fig. 2, can be used to predict when the operator will adopt a crossover-regressive strategy. For example, the limit suggests that regression will also occur for rate control dynamics when the forcing-function bandwidth exceeds 4.0 rad/s.

McRuer et al. [1] explained the effect of crossover regression with normalized mean-squared error (NSME) variation [1] and closed-loop input-to-error spectra [13]. The first rationale, integrating the closed-loop input-to-error spectrum on the basis of the COM, is shown in Fig. 3. It varies the normalized mean-squared error σ_e^2/σ_i^2 with the crossover frequency and eight different bandwidth values. The latter two are normalized by the COM effective time delay τ_e^{com}.

For bandwidths below $0.8\omega_c\tau_e^{\text{com}}$, the optimal performance point is always located at the stability limit, corresponding to a phase margin of 0 deg. For higher bandwidths, the mean-squared error can become larger than 1.0, and optimal performance is obtained by reducing ω_c. In fact, Fig. 3 indicates that optimal performance is then obtained at zero crossover frequency, corresponding to the operator releasing the control manipulator.

The second rationale is illustrated in Fig. 4. The figure is based on the COM, with rectangular-spectrum forcing function having power at all frequencies up to the bandwidth frequency. Two closed-loop input-to-error spectra are compared on a linear scale. When the forcing-function bandwidth approaches the crossover frequency, the shaded area under the curve, which is proportional to the mean-squared error, is smaller for the regressed situation. In the regressed condition, the operator adopts a lower gain and ignores high-frequency input components to reduce the mean-squared error [13]. Note that Fig. 4 contains an inconsistency: the regressive curve never intersects the unity gain line, which is only possible when the time delay is zero.

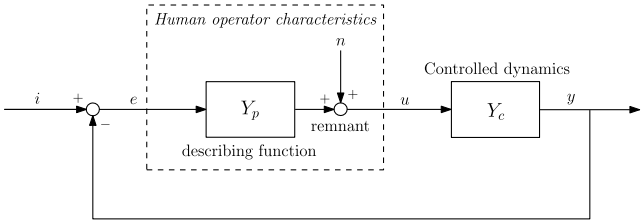

Fig. 1 Quasi-linear human-operator model comprising a describing function and remnant [1].

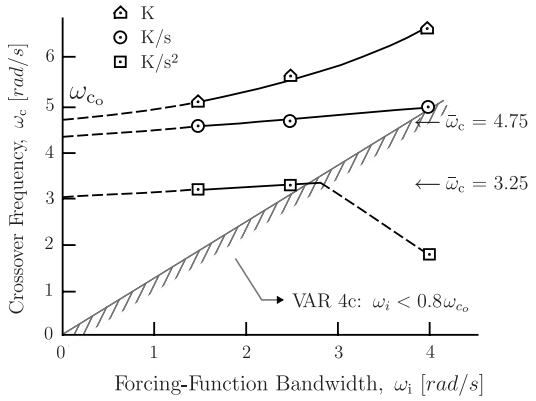

Fig. 2 Dependency of the crossover frequency on controlled element dynamics and forcing-function bandwidth (reproduced from McRuer and Jex [13]).

III. Theoretical Analysis of Crossover Regression

When taking the compromise between performance and stability as a starting point, it is plausible that the cause of crossover regression is from time-delay constraints. In the following, we will investigate which type of control behavior yields minimal closed-loop mean-squared errors. The analysis will provide insight into the effect of the crossover frequency and effective time delay on error reduction. A two-parameter expression is derived that describes the control-behavior adjustment for error minimization in the critical frequency region. Considering this expression with an accurate operator model, a general explanation for the cause of crossover regression can be formulated. The operator models used in this analysis will be introduced first.

**Conditons B7, B8, B9, and B10, having rectangular power spectra of adjacent, equally wide frequency-spaced blocks. The upper frequency (bandwidth) and lower frequency of these blocks were: B7 (0–3.02 rad/s), B8 (3.02–6.03 rad/s), B9 (6.03–9.05 rad/s), and B10 (9.05–12.06 rad/s) [11].

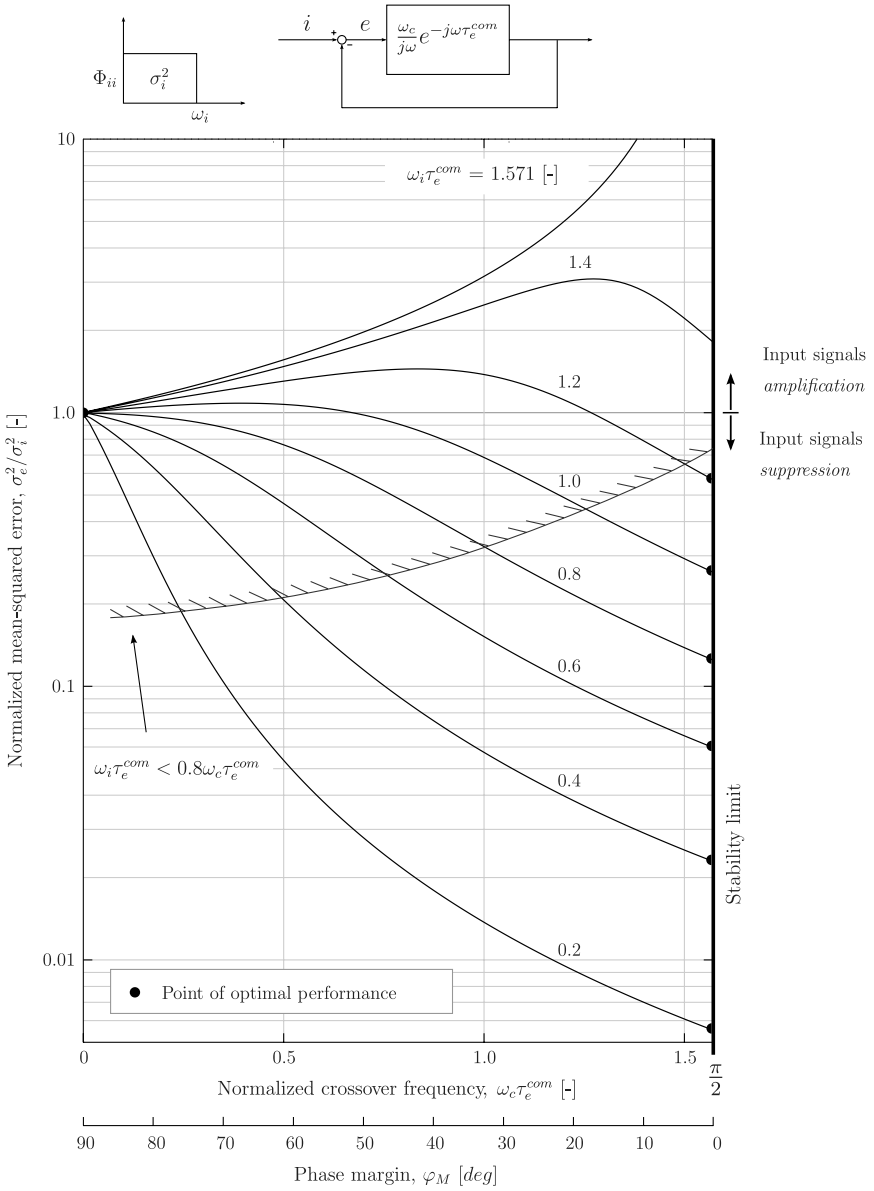

Fig. 3 NMSE for rectangular-spectrum forcing functions (reproduced from McRuer et al. [1]).

A. Human-Operator Modeling

The precision model [1] (PM) approximates linear-operator dynamics in the crossover region, plus the limb/manipulator neuromuscular dynamics††:

$$Y_p^{\text{pm}}(j\omega) = \overbrace{\underbrace{K_p}_{\text{gain}}\underbrace{\frac{(\tau_L j\omega+1)}{(\tau_I j\omega+1)}}_{\text{lead-lag}}}^{\text{equalization}}\underbrace{e^{-j\omega\tau_d}}_{\text{pure time dealy}}\overbrace{\underbrace{\frac{\omega_{\text{nm}}^2}{(j\omega)^2+2\zeta_{\text{nm}}\omega_{\text{nm}}j\omega+\omega_{\text{nm}}^2}}_{\text{neuromuscular dynamics}}}^{\text{limitations}} \tag{3}$$

The simplified precision model (SPM) is only valid near the crossover region and includes the basic equalization and effective time delay [1]:

$$Y_p^{\text{spm}}(j\omega) = K_p\frac{(\tau_L j\omega+1)}{(\tau_I j\omega+1)}\underbrace{e^{-j\omega\tau_e^{\text{spm}}}}_{\text{effective time delay}} \tag{4}$$

It is important to distinguish between the various definitions of operator time delays and the nature of lumped phase-lag contributions. In order of successively more lumped phase-lag contributions, these forms are as follows: the PM pure time delay τ_d; the SPM effective time delay τ_e^{spm}, which lumps the PM delay with phase lags from the neuromuscular dynamics; and the COM effective time delay τ_e^{com}, which lumps the SPM effective time delay with the equalization phase contributions. Clearly, $\tau_e^{\text{com}} \geq \tau_e^{\text{spm}} > \tau_d$.

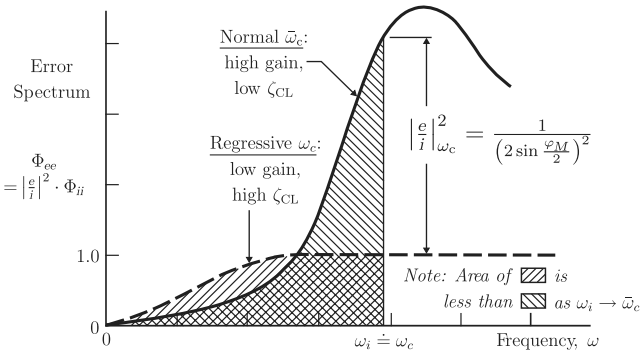

Fig. 4 Explanation of the effect of crossover regression for rectangular-spectrum forcing functions (reproduced from McRuer and Jex [13]).

††The very low-frequency neuromuscular system dynamics were omitted here [1].

Remnant is modeled by filtered Gaussian noise. It can be attributed to perception inaccuracies and thresholds, variations in muscle tension, inabilities to translate motor commands to precise control actions, and time-varying control behavior [1,13–17]. A typical remnant power spectral density is constant at low frequencies and shows a first-order roll off [13,14,18,19]. The remnant power spectral density $\Phi_{nn}(\omega)$ is injected into the closed loop after the operator's describing function (see Fig. 1):

$$\Phi_{nn}(\omega) = \left| \frac{K_n}{1 + \tau_r j\omega} \right|^2 \tag{5}$$

In the following analysis, the cutoff frequency is set to 4 rad/s [13,14,19]. The remnant gain K_n is adjusted to obtain a remnant power σ_n^2 that equals 10% of the total control signal power σ_u^2. This corresponds to remnant intensities as reported in the literature [18,20–22].

B. Effect of Crossover Frequency on the Mean-Squared Error

The advantage of regressing the crossover frequency has become clear from the mean-squared error variation with crossover frequency (Fig. 3). In this analysis, it was assumed that the remnant was zero and that the rectangular forcing-function spectrum had no power content in and beyond the crossover region. Forcing functions in the STI and current experiments, however, consist of sum-of-sinusoids that also have (attenuated) power *beyond* the forcing-function bandwidth ω_i. These sinusoid components are required to identify human control behavior at the frequencies beyond the forcing-function bandwidth.

Figure 5 shows a normalized mean-squared error variation plot, produced by combining the SPM with sum-of-sinusoids forcing functions that have power beyond the bandwidth frequency ω_i, attenuated 20 dB. The controlled dynamics were first-order, because this controlled dynamics requires no equalization. The effects of remnant were again neglected.

Figure 5 illustrates that the best performance always corresponds with mean-squared error values below 1.0. The general shape of the curves for low bandwidth values, that is, $\omega_i \tau_e^{\text{spm}} < 1.0$, resembles that of an inverted umbrella. The sudden growth at smaller phase margins indicates the resonance effects of high-frequency sinusoids. Apparently, the sinusoids beyond the bandwidth frequency ω_i predominate the mean-squared error values for combinations of high crossover frequencies and small (<10 deg) phase margins.

The steady increase in the crossover frequencies that yield optimal performance before the onset of crossover regression corresponds well with the STI findings for this type of forcing functions [1]. Moreover, after crossover regression occurred, the crossover frequencies that yield optimal performance are more realistically located at (very) low frequencies, rather then being zero, which would correspond to the operator releasing the stick.

The most important conclusion from Fig. 5 is still the same as for the rectangular forcing function in Fig. 3. That is, when the normalized bandwidth exceeds $0.8\omega_c\tau_e^{\text{spm}}$, a reduction of the crossover frequency is necessary to warrant optimal performance when ω_i increases. In Fig. 5, crossover regression is evidently not an issue of stability, because the phase margin is always positive. For a fixed time delay, this implies that, at some point, only a crossover-frequency reduction yields the lowest mean-squared error. The required crossover-frequency reduction could very well be a result of

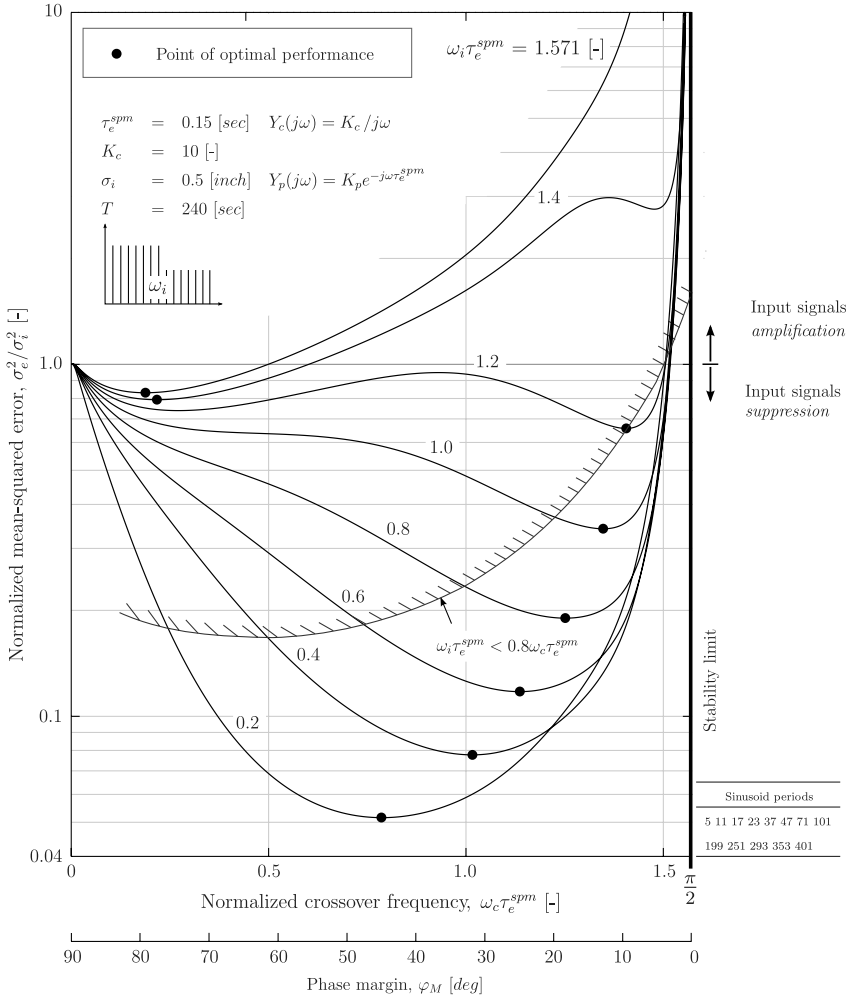

Fig. 5 Refined NMSE variation; sum-of-sinusoids forcing functions with −20 dB attenuated power beyond ω_i.

a limitation in the operator's ability to reduce the SPM effective time delay.

C. Closed-Loop Error Minimization

To minimize NMSE, at some point a crossover-frequency decrease is required. An expression for the closed-loop error power spectrum can be derived from Fig. 1, under the assumption that the forcing-function signal, i, and remnant signal, n, are uncorrelated:

$$\underbrace{\Phi_{ee}(\omega)}_{\text{error spectrum}} = \underbrace{\left|\frac{1}{1+Y_p(j\omega)Y_c(j\omega)}\right|^2}_{\text{input-to-error describing function, }\Phi_{ie}(\omega)} \underbrace{\Phi_{ii}(\omega)}_{\text{input spectrum}} + \underbrace{\left|\frac{-Y_c(j\omega)}{1+Y_p(j\omega)Y_c(j\omega)}\right|^2}_{\text{remnant-to-error describing function, }\Phi_{ne}(\omega)} \underbrace{\Phi_{nn}(\omega)}_{\text{remnant spectrum}} \tag{6}$$

When only the error component due to the forcing function is considered, minimizing the closed-loop input-to-error over all frequencies implies that

$$\Phi_{ie}(\omega) = \left|\frac{1}{1+Y_p(j\omega)Y_c(j\omega)}\right|^2 = \left|\frac{e}{i}\right|^2 < 1 \quad \forall\ \omega \tag{7}$$

Feedback systems containing time delays, such as biological systems, always have frequency ranges that are amplified due to resonance. The error reduction condition of Eq. (7) is therefore not met at all frequencies. Which frequencies are suppressed and which are amplified becomes evident by examining the closed-loop input-to-error spectra in Fig. 6.

The figure is based on the COM and illustrates the effect of typical values for the crossover frequency and effective time delay. Whereas a decrease in effective time delay is always advantageous, the benefit of a decrease in crossover frequency depends on the forcing-function spectrum. For a forcing function with low-frequency sinusoids, a high crossover frequency is beneficial; for a forcing function with sinusoids in the amplification region, a low crossover frequency is beneficial. Figure 6b also shows that, for a zero time delay, the low-frequency sinusoids are suppressed without amplification at any frequency. This shows that the amplification of the power content originates *exclusively* from the effective time delay, although the magnitude of the amplification depends on a combination of the crossover frequency and the effective time delays.

A detailed analysis of the contribution of each sinusoid component to the mean-squared error, for typical examples of SPM parameters, is shown in Fig. 7. These spectra are created with the simplified precision model, $Y_p(j\omega) = K_p e^{-j\omega\tau_e^{\text{spm}}}$, controlled element dynamics, $K_c/j\omega$ with K_c of 5, the remnant spectrum of Eq. (5), and STI 8-2 spectrum forcing function. It shows that the forcing-function sinusoid components located near the maximum closed-loop input-to-error amplification frequency are the main cause of the mean-squared error, for both nonregressed (Figs. 7a and 7b) and regressed (Figs. 7c and 7d) operators. In the remainder, the frequency range near the maximum closed-loop input-to-error amplification region, or, more specifically, the frequencies just above ω_c, will be referred to as center frequencies. To achieve the optimum performance, the operator will attempt to minimize the sinusoids' power at these center frequencies while retaining effective suppression of low-frequency sinusoids.

An accurate expression of the maximum closed-loop input-to-error amplification ratio might be valuable, as this ratio turns out to be crucial for operator adjustment to obtain minimal mean-squared errors. Considering the Nyquist locus in Fig. 8, the power content at frequencies on the locus traveling through the critical circle is amplified.

The maximum amplification ratio is by definition the shortest distance from the locus to the point $(-1, j0)$. This distance is illustrated in Fig. 8 by $\|M_p\|$. The derivation of an exact expression for this ratio in terms of phase margin φ_M and gain margin (GM) is not possible. Instead, exact expressions for the amplification ratio at gain crossover ω_c and phase crossover ω_{cp} can be derived. These will be used to approximate the desired maximum closed-loop input-to-error ratio.

At gain crossover, the amplification ratio is the shortest distance from the locus, coinciding with the crossover frequency, to the point $(-1, j0)$. Considering the phase margin in radians, McRuer et al. [1] presented the amplification ratio as

$$\left|\frac{e}{i}\right|_{\omega_c} = \left|\frac{1}{\|M_c\|}\right| = \frac{1}{2\sin(\varphi_M/2)} \tag{8}$$

Van der Vaart derived an expression for the amplification ratio at phase crossover [9]

$$\left|\frac{e}{i}\right|_{\omega_{\text{cp}}} = \frac{1}{1-1/\text{GM}} = \frac{1}{1-(2/\pi)\omega_c\tau_e^{\text{com}}} \tag{9}$$

Figure 9 shows that Eq. (9) is the best approximation of the maximum amplification ratio. Note that the frequency at the GM ω_{cp} is always higher than the maximum amplification ratio frequency and, consequently, Eq. (9) always underestimates the amplification ratio. Nevertheless, it is remarkable how well the two-parameter expression of Eq. (9) approximates the ratio. It might be informative about the organization of the operator parameter adjustment (in terms of the COM effective time delays and crossover frequency) with respect to closed-loop error minimization. To gain a better understanding of Eq. (9), the COM effective time delay will be considered in more detail.

D. Crossover Model Effective Time Delay

Operators achieve the best closed-loop performance by minimizing Eq. (9). Several high-frequency phase-lag and lead

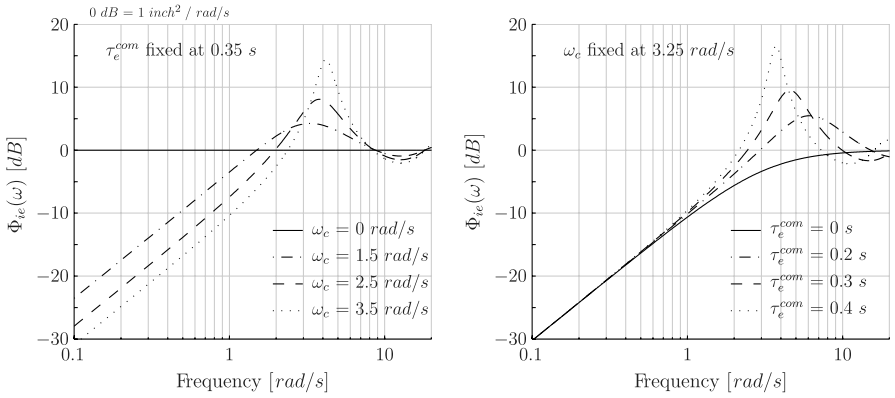

a) Effect of crossover frequency, ω_c **b) Effect of COM effective time delay, τ_e^{com}**

Fig. 6 Closed-loop input-to-error describing function spectra.

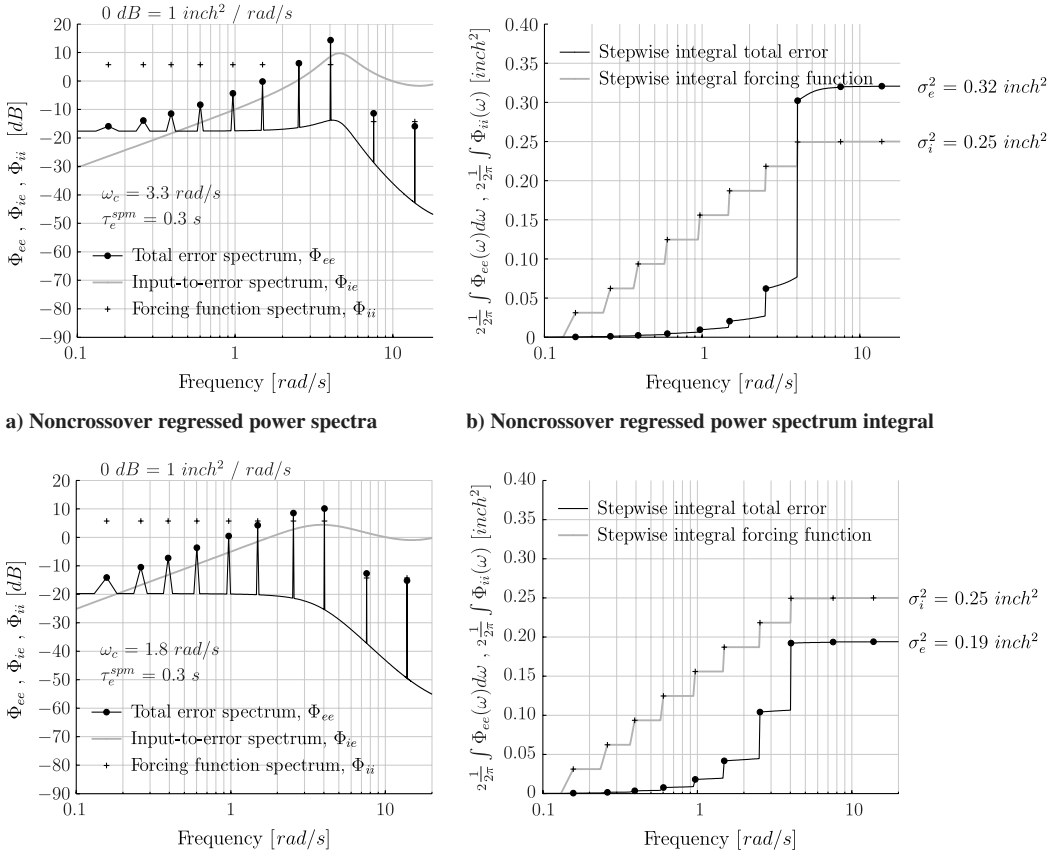

a) Noncrossover regressed power spectra

b) Noncrossover regressed power spectrum integral

c) Crossover regressed power spectra

d) Crossover regressed power spectrum integral

Fig. 7 Closed-loop error, input-to-error, and forcing-function spectra.

contributions are lumped into the COM effective time delay at crossover. Assuming that the PM is the most accurate control-behavior representation at all frequencies, the open-loop phase lag becomes

$$\varphi(\omega) = \angle_{\text{rad}} Y_c - \tau_d \omega - \arctan \frac{2\zeta_{\text{nm}}/\omega_{\text{nm}}}{1-(\omega/\omega_{\text{nm}})^2}\omega - \arctan \tau_I \omega + \arctan \tau_L \omega \tag{10}$$

For a small neuromuscular phase contribution at the center frequencies, the arctangent can be assumed to be equal to its argument, that is, $\arctan x \doteq x$. Furthermore, this term can be simplified to $2\zeta_{\text{nm}}/\omega_{\text{nm}}$ as $(\omega/\omega_{\text{nm}})^2 \to 0$ when $\omega_{\text{nm}} \gg \omega_c$. As long as $\tau_L\omega_c > 1$ and $\tau_I\omega_c > 1$, elegant ways to linearize the arctangents are nonexistent. The phase-lag contributions at center frequencies can be approximated by

$$\Delta\varphi_{\text{center}}(\omega) \doteq \angle_{\text{rad}} Y_c - \omega[\tau_d + 2\zeta_{\text{nm}}/\omega_{\text{nm}}] - \arctan \tau_I \omega + \arctan \tau_L \omega \tag{11}$$

From Eq. (11), a general expression of the COM effective time delay can be derived:

$$\tau_e^{\text{com}} \doteq \tau_d + \underbrace{2\zeta_{\text{nm}}/\omega_{\text{nm}}}_{\text{limb-manipulator neuromuscular dynamics}} + \underbrace{(-\pi/2 - \angle_{\text{rad}} Y_c - \arctan \tau_L\omega_c + \arctan \tau_I\omega_c)/\omega_c}_{\text{equalization adjustment}} \tag{12}$$

For the three basic types of controlled element dynamics, the COM effective time delays can now be defined. Note that, when the

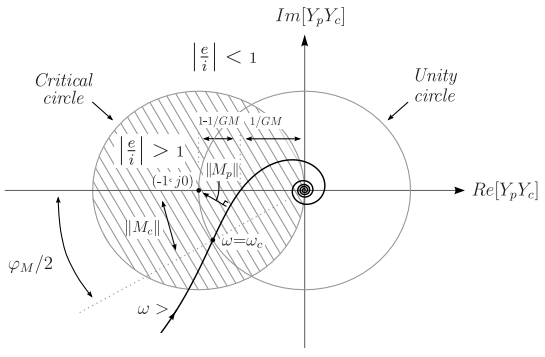

Fig. 8 Geometric derivation of maximum input-to-error amplification expressions from the open-loop Nyquist representation.

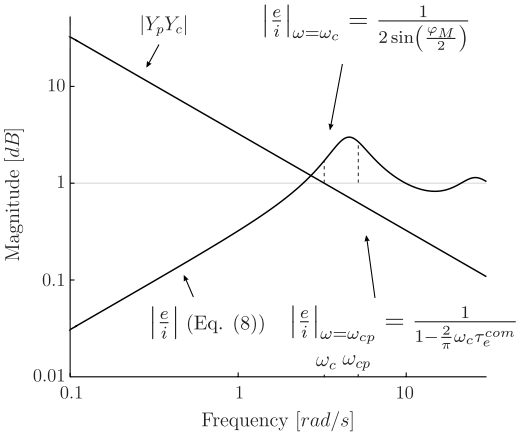

Fig. 9 Expressions for $|e/i|_{\max}$, closed-loop input-to-error and open-loop magnitude responses.

lead- and lag-time constants become very large, the COM effective time delay approximates Eq. (14) for all dynamics:

Proportional control dynamics

$$\tau_e^{\text{com}} \doteq \tau_d + 2\zeta_{\text{nm}}/\omega_{\text{nm}} - \underbrace{[\pi/2 - \arctan \tau_I \omega_c]/\omega_c}_{\text{lag equalization}} \tag{13}$$

Rate control dynamics

$$\tau_e^{\text{com}} = \tau_e^{\text{spm}} \doteq \tau_d + 2\zeta_{\text{nm}}/\omega_{\text{nm}} \tag{14}$$

Acceleration control dynamics

$$\tau_e^{\text{com}} \doteq \tau_d + 2\zeta_{\text{nm}}/\omega_{\text{nm}} + \underbrace{[\pi/2 - \arctan \tau_L \omega_c]/\omega_c}_{\text{lead equalization}} \tag{15}$$

Now that the different contributions to the COM effective time delay are known, the adjustment of the human operator to achieve minimal mean-squared errors can be evaluated.

E. Generalizing the Cause of Crossover Regression

Minimization of the mean-squared error is obtained by a value of the crossover frequency that exceeds the forcing-function bandwidth, yet causing not too much resonance of forcing-function power content at center frequencies. The magnitude of the two-parameter equation, Eq. (9), should therefore remain within reasonable bounds. This is effectively achieved by minimizing the COM effective time delay, that is, minimize the pure time delay and both equalization and neuromuscular contributions, Eqs. (13–15).

The pure time delay accounts for time delays due to perception, cognition, conduction within the cortex, and neural conduction from cortex to limb [1], but also depends on the type of controlled dynamics and the nature of the task. Acceleration control, for instance, requires the operator to estimate velocity with an associated time-delay penalty of roughly 14 ms, as given by the verbal adjustment rules [1]. Time delays due to the nature of the task can stem from various sources, such as additional time delays in divided attention tasks [6].

Minimizing the equalization contribution is achieved by increasing the lead τ_L and decreasing the lag τ_I. The limb-manipulator neuromuscular dynamics are likewise adjusted to provide minimal neuromuscular phase lag at crossover. Minimization of the neuromuscular contribution, however, depends to some extent on task-related characteristics. That is, faster forcing-function signals require faster and more agile stick maneuvers, resulting in lower neuromuscular damping and less phase lag at crossover.

Because of physical and mental limitations, at some point, the COM effective time delay cannot decrease anymore, that is, a further reduction is beyond human capabilities. If a human operator wants to reduce the resonance peak even further, he can only do so by lowering the crossover frequency. To obtain lower mean-squared errors, the operator must adopt a crossover-regressive control strategy. Crossover regression can therefore be concluded to result primarily from human limitations in sufficiently decreasing the COM effective time delay.

F. Crossover Model Effective Time Delays in the 1965 STI Experiment

The SPM effective time delays in the STI experiment, illustrated in Fig. 10, were obtained by fitting the SPM to experimental data [1]:

$$\varphi_{M_{\text{rad}}} = \frac{\pi}{2} - \omega_c \tau_e^{\text{com}} \tag{16}$$

The COM and SPM effective time delays, measured in the STI experiment, are illustrated in Fig. 11. The COM effective time delay was calculated by rearranging Eq. (16) and substituting the crossover frequency and phase margin.[‡‡] Additionally, two distinct upper limits on the COM effective time delay are included in Fig. 11.

[‡‡]Phase margins and crossover frequencies obtained from McRuer et al. [1], Table 8, p. 149.

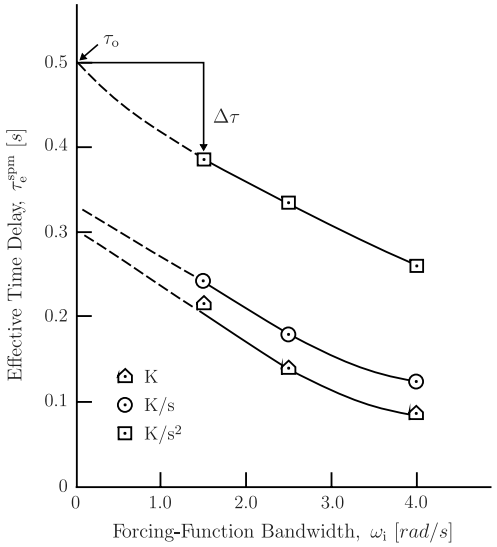

Fig. 10 Variation of effective time delay with forcing-function bandwidth and controlled element dynamics (reproduced from McRuer and Jex [13]).

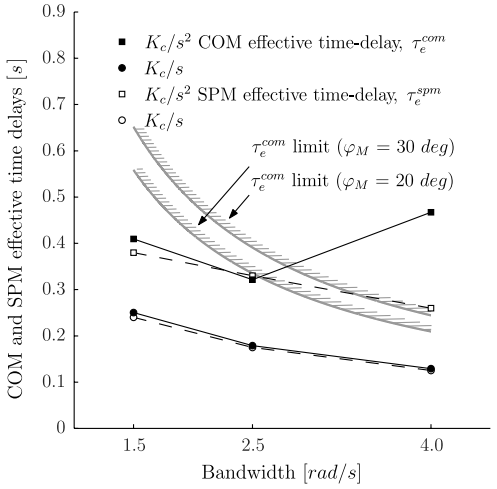

Fig. 11 COM and SPM effective time delays of the 1965 STI experiment [1] and two upper limits.

The limits assume that, under normal tracking conditions, a phase margin between 20 and 30 deg is desirable. Because an exact value of the desired phase margin is unknown, limits for both a phase margin of 20 and 30 deg are depicted. To calculate these limits, it was further assumed that the baseline crossover frequency ω_{c_0} approximately equaled the crossover frequency. Combining Eqs. (2) and (16) now defines an upper limit on the COM effective time delay as a function of forcing-function bandwidth. To prevent crossover regression, while maintaining the selected stability margin, the COM effective time delay should remain above or at the limit.

For acceleration control, the 2.5 rad/s bandwidth condition is below both limits, although the 30 deg phase-margin limit is close. Indeed, McRuer et al. [1] found no crossover regression for this condition. Crossover regression, together with an increase in COM effective time delay, was found with acceleration control and 4.0 rad/s forcing-function bandwidth. The SPM effective time delay in Fig. 9 decreases for this condition. This leads to two observations: First, the increase in COM effective time delay was due to an increase in the equalization contribution, associated with a decrease in the crossover frequency, Eq. (15). Second, Fig. 10 shows that crossover regression does not prevent the operator from exploiting those forcing-function characteristics that allow a further decrease in SPM effective time delay.

Based on the analyses and observations, it was hypothesized that the COM effective time delay could not decrease sufficiently to reduce the magnitude of Eq. (9) sufficiently and the crossover frequency decreased instead. To investigate the adjustment of the COM effective time delay, explore the adjustment, between-subject variation, and accuracy of PM parameters in relation to crossover regression, an experiment was conducted.

IV. Experiment

The experiment was designed with three objectives in mind: 1) To replicate the 1965 STI experiment as well as possible, to obtain accurate, established reference values of manual control behavior, 2) to explore the COM effective time delay just before the occurrence of crossover regression, and 3) to study the trends, between-subject variation, and accuracy of the PM parameter estimates in both regressive and nonregressive conditions.

A. Experiment Setup and Procedure

To replicate the 1965 STI experiment, a compensatory tracking task with a central foveal display was set up in our human-machine systems laboratory (Fig. 12). The controlled dynamics were a pure acceleration control $K_c/(j\omega)^2$ selected for two reasons. First, for these dynamics, the STI experiment results yield reference values of control behavior in conditions where crossover regression did and did not occur. Second, crossover regression has primarily occurred with this type of dynamics [8–10]. The controlled dynamics gain K_c was fixed at 5 in./in.

Fig. 12 Experimental setup showing display and side stick.

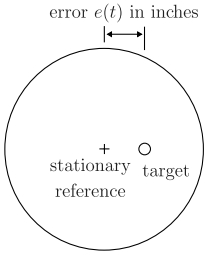

Fig. 13 Display layout equivalent to the STI display [1].

The control manipulator was an electrohydraulic, servo-controlled, passive sidestick with 1 deg of freedom (lateral). The moment arm was 9 cm. The spring-restrained sidestick dynamics were similar to the STI experiment; the torsional stiffness K_s was 3.5766 Nm/rad, while torsional damping B_s and mass M_s were kept as low as possible at 0.08 Nm s/rad and 0.01 kg m^2, respectively.

Participants were seated in an adjustable chair in a low-noise, darkened room. They were asked to keep the eye-to-display distance constant at approximately 29 in. Participants were presented a one-dimensional display, Fig. 13, showing a stationary reference (cross) fixed at the center of the screen and a target (circle) that moved laterally. The stationary reference and target were displayed in green on a black background. The display size and layout exactly matched the STI display; the frame of reference was inside out, implying that the reference (cross) had to be directed toward the target (circle).

The experiment comprised two phases:

1) *Training phase.* Participants were allowed to become accustomed to the experimental apparatus and tasks. The conditions were divided into four categories: easy, baseline, medium, and difficult; these will be further discussed later. For each category, it was determined what type of control strategy yielded the lowest normalized tracking error $\bar{e}^2/\sigma_i^2$. At the end of this phase, reasonable levels of stationary tracking performance were obtained using the selected control strategy, expressed in $\bar{e}^2/\sigma_i^2$ and also control activity $\bar{u}^2$. Participants performed an average of 120 training trials.

2) *Measurement phase.* The data of five successive runs for each condition were recorded for evaluation.

The experimental design consisted of randomizing all conditions. To minimize changes in the control strategy during measurement runs, each condition was announced before each run, so that the participant could associate the nature of the run with the selected control strategy in the training phase.

B. Independent Variables

The independent variable in the experiment was the forcing function. Five distinct forcing-function conditions were used (see Fig. 14).

The reference conditions were the three STI spectrum forcing functions with 1.5, 2.5, and 4.0 rad/s bandwidth (conditions A, B, and D, respectively), extended with two additional conditions (C and E). To prevent fatigue, to obtain high levels of stationary control behavior, and to maintain sufficient frequencies without power around the low-frequency sinusoids, the runs lasted 108 s instead of the 240 s in the STI experiment. Hence, the number of periods of the original STI forcing functions had to be divided by approximately two. The periods were selected as integer multiples of the base frequency $2\pi/T$, but were not allowed to be integer multiples of each other [23]. Our frequencies therefore only approximated those of the STI experiment (see Table 1).

The first additional condition, C, was a forcing function with bandwidth 3.0 rad/s. An additional sinusoid was added to obtain this bandwidth; to maintain an approximately equal logarithmic frequency separation, some periods were slightly changed. Condition C was added for two reasons: first, to provide an insight into human control behavior, and in particular into the crossover model effective time-delay just before crossover regression is expected to occur.

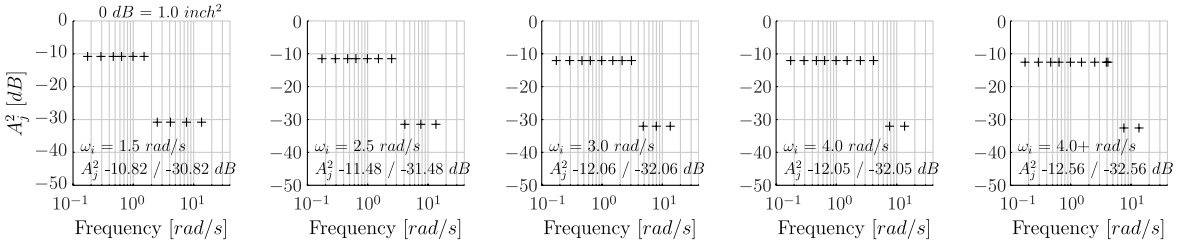

a) Cond. A (STI 6-4) b) Cond. B (STI 7-3) c) Cond. C d) Cond. D (STI 8-2) e) Cond. E

Fig. 14 Definition of power spectra magnitudes. All forcing functions are normalized to σ_i of 0.5 in.

Table 1 Definition of forcing-function periods and harmonic frequencies

Conditions A, B, and D STI forcing functions				Condition C Bandwidth frequency sinusoids			Condition E High-frequency sinusoids		
j	Period, –	ω_j, rad/s	STI ω_j, rad/s	j	Period, –	ω_j, rad/s	j	Period, –	ω_j, rad/s
1	3	0.175	0.157	1	3	0.175	1	3	0.175
2	5	0.291	0.262	2	5	0.291	2	5	0.291
3	8	0.465	0.393	3	8	0.465	3	8	0.465
4	11	0.640	0.602	4	11	0.640	4	11	0.640
5	17	0.989	0.969	5	17	0.989	5	17	0.989
6	26	1.51	1.49	6	26	1.51	6	26	1.51
7	43	2.50	2.54	7	**37**[a]	**2.15**	7	43	2.50
8	71	4.13	4.03	8	**53**	**3.08**	8	**67**	3.90
9	131	7.62	7.57	9	**83**	**4.83**	9	71	4.13
10	233	13.56	13.8	10	**137**	**7.97**	10	131	7.62
				11	233	13.56	11	233	13.56

[a]Bold font indicate the differences with respect to the STI forcing-function periods.

The second reason is to investigate the between-subject variability in the occurrence of crossover regression at 3.0 rad/s.

The second additional condition, E, was a forcing function with a higher level of difficulty than condition D (STI 8-2). This was achieved by adding an additional sinusoid to condition D, just before the 4.0 rad/s bandwidth frequency. The additional sinusoid was inserted close to the maximum closed-loop input-to-error amplification frequency (see Fig. 6). This condition served to better investigate the trends in human control behavior in regressive conditions.

The categories of the conditions were determined based on their expected difficulty level: easy (A), baseline (B), medium (C), and difficult (D and E). In the remainder of this paper, the five forcing-function conditions are identified by their bandwidth. Condition E differs from condition D only by addition of a '+' symbol to the bandwidth, that is, 4.0+.

C. Participants and Instructions

Five participants were selected primarily on the basis of having excellent tracking skills to match the performance of the STI experiment population. The participants were instructed to keep the reference as close as possible to the target, i.e., to minimize the error e. Their motivation was enhanced by actively keeping track of personal mean-squared error records and by provoking a competition among the participants.

For each 108-s run, 10 s run-in time and 2 s run-out time were added. Of the 10 s run-in time, the first 5 s featured a ramp-shaped fade-in to smoothen the participant's transition from inactivity to active tracking.

D. Limitations in Replicating the 1965 STI Experiment

Some aspects could not be exactly replicated. Whereas the STI experiment featured an analogue cathode ray tube display [13], we used a low-latency, high-resolution liquid crystal display. Second, no mention is made in the 1965 report of the stick grip. A later 1974 STI report [7] mentions an experiment very similar to the 1965 experiment, in which the stick was "grasped between thumb and forefinger." In our experiment, the stick was grasped with the full hand. Third, whereas the STI participants had extensive piloting experience, none of our participants did.

E. Human Control-Behavior Identification

The operator describing function was identified from the experimental data using two different nonparametric techniques. In addition, the precision model parameters were estimated using a parametric identification technique. The identification methods are briefly reviewed next.

1. *Nonparametric Identification*

Two methods were used to obtain describing functions from the measured data. First, the Fourier coefficients (FC) method was applied to obtain an estimate of the frequency response function at the frequencies of the forcing-function sinusoids [1,23,24]; at these frequencies, high signal-to-noise ratios are feasible. Second, the auto-regressive with exogenous inputs model (ARX) method was used [25]. This method fits linear polynomials to time-domain signals by solving an analytical least-squares criterion and yields an estimate of the frequency response function at all frequencies [26,27].

2. *Parametric Identification*

The maximum likelihood estimation (MLE) method was used to estimate the precision model parameters [22,28,29]. The main advantages of this method are that the variance of the parameter estimate achieves the Cramér-Rao lower bound (CRLB) (that is, it is asymptotically efficient), and also that the estimate becomes unbiased (i.e., it is asymptotically unbiased), both when the observation time approaches infinity [22,28]. The principle is to find the joint-probability density function for predicted error ε (the difference between the measured and modeled control signal) that makes the parameter estimate $\hat{\theta}$ "most likely" by maximizing the likelihood function:

$$L(\theta) = f(\varepsilon_1, \varepsilon_1, \ldots, \varepsilon_N; \theta) \tag{17}$$

The parameter vector $\hat{\theta}^{\text{mle}}$ that maximizes the likelihood function is defined by

$$\hat{\theta}^{\text{mle}} = \arg\max_{\theta} \ell_n L(\theta) = \arg\min_{\theta} \frac{1}{2\sigma_\varepsilon^2} \sum_{i=1}^{N} \varepsilon_i^2 \tag{18}$$

The convex Gauss–Newton optimization method used to find the maximum log likelihood unfortunately suffered from local minima. To enhance the probability of finding the global minimum, multiple initial conditions were used. When all the initial conditions converged to the same minimum, a global minimum was assumed.

A measure for the amount of information available in the data set to compute the parameter estimate $\hat{\theta}^{\text{mle}}$ can be obtained by calculating the Fisher information matrix. The inverse of this matrix defines the Cramér-Rao lower bound, that is, the minimum achievable variance of estimate $\hat{\theta}^{\text{mle}}$.

3. *Relative Remnant and Linear Correlation*

The relative remnant ρ_a^2 is a measure for the linearity and model validity [1]. It describes how well the linear precision model fits the data; it ranges from zero to one, where one corresponds to perfectly linear correspondence. It can be calculated by

$$\rho_a^2 = 1 - \frac{(\bar{u} - \bar{u}_m)^2}{\bar{u}^2} = 1 - \frac{\bar{n}^2}{\bar{u}^2} \tag{19}$$

with u_m as the simulated control signal obtained with the PM.

The squared correlation coefficient ρ^2, also known as the coherence squared, is the ratio of the linearly correlated operator control signal power and the total control signal power [1]:

$$\rho^2(\omega) = \frac{|\Phi_{eu}(\omega)|^2}{\Phi_{ee}(\omega)\Phi_{uu}(\omega)} \tag{20}$$

A larger correlation coefficient implies a lower remnant portion at the frequency under consideration; it ranges between zero (only remnant) and one (no remnant).

A typical open-loop estimate, including values for ρ_a^2, is shown in Fig. 15.

F. Dependent Measures

Several metrics for human behavior were investigated. Time-domain performance was expressed using the mean-squared values of the error, control signal, and control signal derivative. Frequency-domain behavior metrics were the crossover frequency, phase margin, and linear precision model parameters. The accuracy of the parameter estimates were expressed in the normalized averaged Cramér-Rao lower-bound values. Metrics used for the level of nonlinearity in operator behavior included the squared linear correlation coefficient ρ^2, the mean-squared remnant $\bar{n}^2$, and the relative remnant ρ_a^2.

G. Hypotheses

Five hypotheses were defined. The first three were based on findings in previous experiments, and the remaining two originate from the theoretical analysis of Sec. III.

First, after the occurrence of crossover regression, the between-subject variability is hypothesized to increase in terms of the crossover frequency (1a), as well as the estimated PM parameters (1b). Second, the accuracy of the PM parameter estimates, expressed in normalized averaged CRLB values, is hypothesized to decrease for regressed conditions. Third, the linearity in operator control behavior is hypothesized to decrease when crossover regression occurs. Fourth, the COM effective time delay is hypothesized to increase after the occurrence of crossover regression. Fifth, the maximum closed-loop input-to-error ratio is hypothesized to decrease after crossover regression occurs.

V. Results

The statistical significance of the effects of the forcing functions on the dependent measures was determined by a repeated-measures analysis of variance (ANOVA). An ANOVA makes four assumptions regarding the underlying data set: 1) normality, 2) homogeneity of variance, 3) sphericity, and 4) interval scale. Because only one group of participants was considered, the assumption of homogeneity of variance was always true. Although an ANOVA can be quite robust against violations of the normality assumption [30,31], the nonparametric Friedman ANOVA was used instead when the data appeared to be nonnormal.

In the figures that follow, the 4.0+ condition is offset from the 4.0 rad/s condition on the abscissa. The offset marks the hypothesized increase in task difficulty.

A. Time Histories

Time histories of the closed-loop input (equal to reference i) and output (equal to controlled element response y) are illustrated in Fig. 15, for both regressed and nonregressed participants. Typical tracking performance in following the 2.5 rad/s forcing function is illustrated by participant 2: the reference could be tracked reasonably well. The time-history of the 4.0 + rad/s forcing-function reference was clearly more volatile due the additional power at center frequencies. In response, all participants decreased their crossover frequency.

Generally, two types of crossover-regressive strategies were adopted by the participants, typical examples are shown in Fig. 16. Participant 5 regressed the crossover frequency to 1.1 rad/s and completely ignored the high-frequency parts of the signal. Participant 4 tried to follow the high-frequency input more closely and adopted a slightly higher crossover frequency, 1.7 rad/s. The latter participant was unable, however, to sufficiently compensate for his inherent time delay, and his response was almost continuously out of phase. More results will be discussed next, in the same order as the hypotheses were defined.

B. Hypothesis 1: Between-Subject Variability

1. Time-Domain Metrics

The means and 95% confidence intervals (CI), adjusted for between-subject variability, of time-domain tracking performance are given in Fig. 17. The ANOVA results are given in Table 2. Reference values of the mean-squared (MS) control deflection could not be found in the 1965 STI report; therefore, values from an almost identical STI experiment reported in 1966 by Wasicko et al. [32] were taken as a reference. Note, however, that the latter experiment featured only one participant.

An almost linear increase in the normalized mean-squared error can be observed in Fig. 17a. Mean-squared control activity, Fig. 17b, increases up to 3.0 rad/s and then decreases again. The trend in the control deflection derivative, Fig. 17c, is quite similar. All effects were significant (see Table 2).

The values found are very similar to those reported by McRuer et al. [1], providing confidence that we were indeed successful in replicating their experiment. Marked exceptions are the worse performance of our participants in reducing the NMSE for the 4.0 rad/s condition and the much lower MS control activity for the

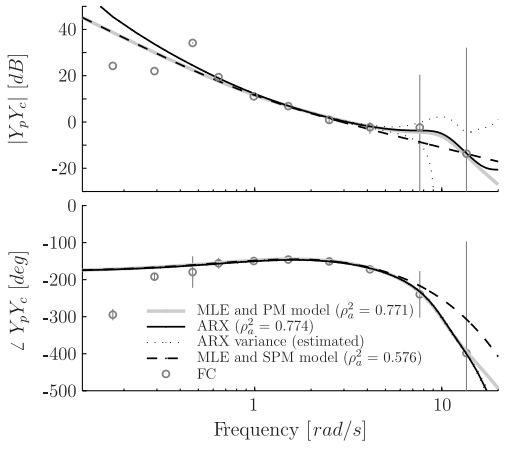

Fig. 15 Open-loop dynamics estimates (1.5 rad/s condition A, participant 1).

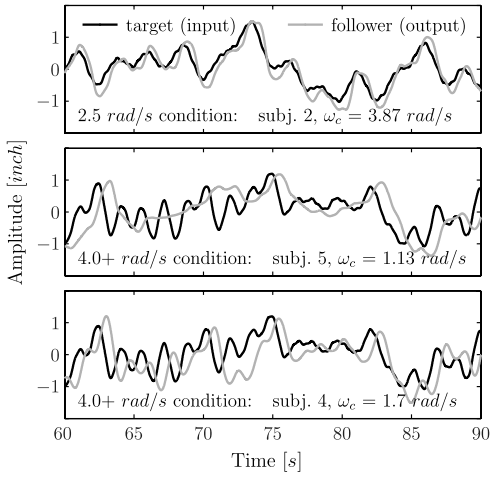

Fig. 16 Typical time histories for regressed and nonregressed participants.

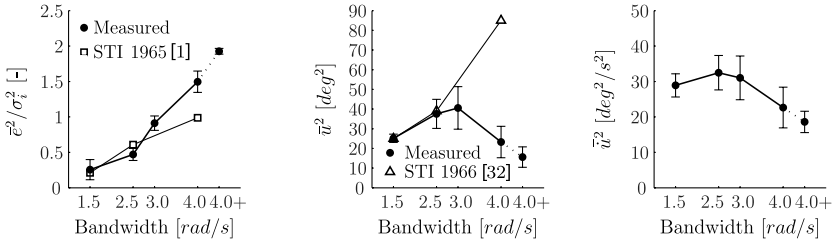

a) Normalized mean-squared error **b) MS control deflection** **c) MS control derivative**

Fig. 17 Means and 95% CI, corrected for between-subject variability.

same condition. Recall, however, that the value reported by Wasicko et al. [32] belonged to just one participant.

The individual NSME and MS control deflections, including group means and standard deviations, are shown in Figs. 18 and 19, respectively. For the 3.0 and 4.0 rad/s conditions, the between-subject variability in NMSE slightly increases. The variations in MS control deflection are much larger, especially for the 3.0 and 4.0 rad/s conditions. Although MS control activity was considerably higher for participants 1 and 4, their NMSE performance was about the same (participant 4) or only slightly better (participant 1).

2. *Frequency-Domain Metrics*

The crossover frequencies, phase margins, and closed-loop damping ratio are shown in Fig. 20. The ANOVA results can be found in Table 2.

The crossover frequency increases slightly for bandwidths up to 2.5 rad/s and then becomes considerably smaller. Apparently, crossover regression occurred first in the 3.0 rad/s condition. The phase margin increases almost proportionally with forcing-function bandwidth, Fig. 20b. The closed-loop damping, Fig. 20c, remains at approximately 0.2 for the 1.5 and 2.5 rad/s conditions and then increases to roughly 0.45 for both the 4.0 and 4.0 + rad/s conditions. These effects were all significant.

As compared to the original STI experiment, the crossover frequencies were considerably higher for the 1.5 and 2.5 rad/s conditions; the phase margin shows only slight differences. The trends in the data, however, were exactly the same in our experiment.

Notice that the trends in crossover frequency and MS control deflection are similar, a significant effect (correlation coefficient 0.9285, $p = 0.0227$); the same holds when comparing the NMSE and phase-margin trends, an effect that is not significant (correlation coefficient 0.7240, $p = 0.1667$). This indicates that performance in terms of minimizing error is related to phase margin, rather than crossover frequency. The latter is a better (but not significant) predictor of the MS control activity.

Figure 21 shows the average crossover frequencies of each individual participant, with group means and standard deviations. Examination of the individual crossover frequencies reveals considerable variations. The first regression can be noticed at the 3.0 rad/s condition, for participants 2 and 5. Participant 3 regresses at the 4.0 rad/s condition. Participants 1 and 4 also regress at this condition, but to a lesser extent; they further reduce their crossover frequency at the 4.0+ condition. Overall, the between-subject variability in crossover frequency increases after the 2.5 rad/s condition. This observation supports hypothesis 1(i); between-subject variability in crossover frequency increases when crossover regression effects start to occur.

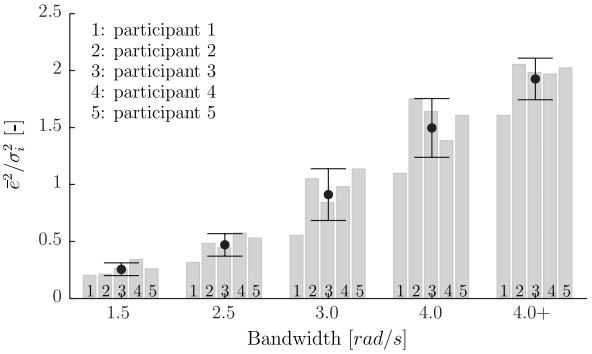

Fig. 18 Individual NMSE, means, and standard deviations.

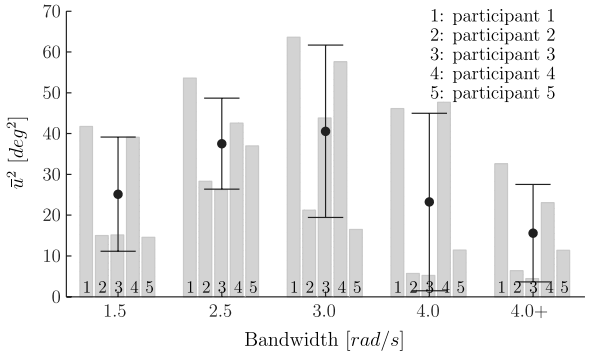

Fig. 19 Individual MS control deflection, means, and standard deviations.

Regarding the crossover frequencies beyond the 3.0 rad/s condition, two groups can be distinguished: participants 1 and 4, who maintain a relatively high crossover frequency (between 1.7 and 2.4 rad/s), and participants 2, 3, and 5, who adopt a lower crossover frequency (approximately 1.1 rad/s). The variability in crossover frequency is confined to a tight band for the 2.5 rad/s condition, followed by the 1.5 rad/s and 4.0+ conditions.

Table 2 Results of repeated-measures ANOVA on performance and frequency-domain behavior metrics, where ∗∗ is highly significant ($p < 0.01$) and ∗ is significant ($0.01 \leq p < 0.05$)

Independent variable	Dependent measures									
	Time-domain performance				Frequency-domain behavior					
	$\bar{e}^2/\sigma_i^2$		$\bar{u}^2$		ω_c		φ_M		ζ_{CL}	
	$\chi^2(4)$	Sig.	$\chi^2(4)$	Sig.	F(4, 16)	Sig.	F(4, 16)	Sig.	$\chi^2(4)$	Sig.
Bandwidth	20.0[a,b]	∗∗	15.520[a]	∗∗	53.705	∗∗	12.395	∗∗	10.4[a,b]	∗

[a]Sphericity assumption not met, Friedman's ANOVA used instead.
[b]Sphericity assumption not met.

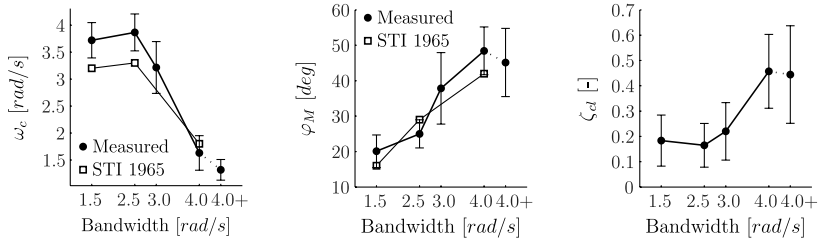

a) Crossover frequency **b) Phase margin** **c) Closed-loop damping**

Fig. 20 Means and 95% CI, corrected for between-subject variability.

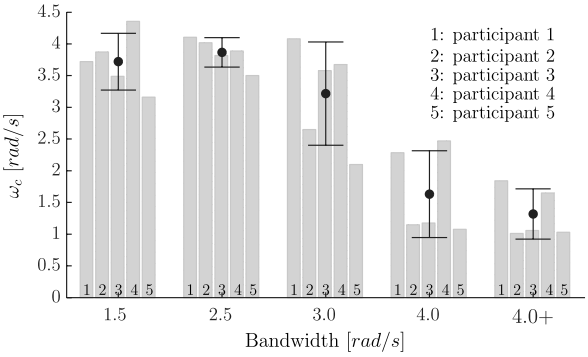

Fig. 21 Individual crossover frequencies.

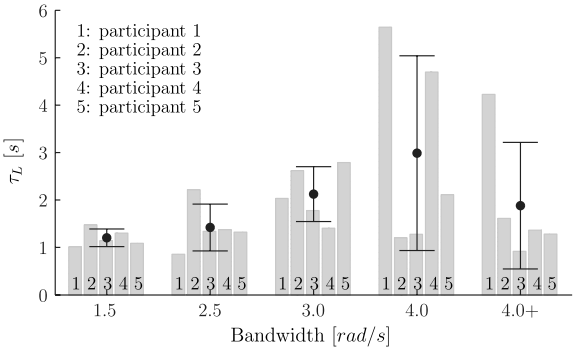

Fig. 23 Individual lead-time constants.

3. Precision Model Parameter Estimates

The precision model parameters, means, and 95% confidence intervals are illustrated in Fig. 22; ANOVA results are summarized in Table 3. With double integrator dynamics, no lag equalization is needed, and the lag-time constant τ_l in Eq. (3) was set to zero.

The following trends can be observed from Fig. 22. The operator gain K_p is approximately the same (0.52) for the 1.5 and 2.5 rad/s conditions, then decreases considerably to an again approximately constant level (0.15) in the 4.0 and 4.0 + rad/s conditions. The pure time delay τ_d decreases almost proportionally with forcing-function bandwidth and becomes even slightly lower in the 4.0 + rad/s condition. These effects are indeed significant (see Table 3).

The lead-time constant τ_L increases for higher forcing-function bandwidths and then drops again for the 4.0+ condition. Overall, the variability in lead generation is high and, as a result, no significant effects of bandwidth were found.

Inspection of the individual lead-time constants in Fig. 23 provides more information on the adjustment taking place. Participants 2, 3, and 5 show a very similar adaptation, as they all increased their lead up to the 3.0 rad/s condition and then decreased their lead again for the 4.0 and 4.0+ conditions. Participant 1 dramatically increased his lead time for both the 4.0 rad/s and 4.0+ conditions. Participant 4 maintained an approximately equal lead time of 1.3 s for all conditions except the 4.0 rad/s condition, where lead was very much higher.

Tentatively, the sudden increase in lead time for participants 1 and 4, yielding smaller effective time delays, can be interpreted as a "last attempt" of these participants to maintain tracking performance, resisting a total regression of the crossover frequency, as happened with the other three participants. But as mentioned earlier, it did not help them very much, as their NMSE performance was about the same or only slightly better.

The neuromuscular damping ζ_{nm} reduces almost linearly for higher bandwidths, a significant effect. Although, clearly, a reduction is apparent in the neuromuscular frequency ω_{nm}, this effect was not significant. This is probably due to the fact that between-subject variations were higher in the regressive conditions. Recall that in hypothesis 1(ii) we stated that the between-subject variability in the precision model parameters increases after the occurrence of crossover regression. From the parameters discussed, it is clear that this hypothesis only holds for the operator lead time and, to a lesser extent, the neuromuscular frequency.

C. Hypothesis 2: Accuracy of the Precision Model Parameter Estimates

Averaged Cramér-Rao lower bounds, normalized to the parameter magnitudes, are shown in Fig. 24. Note that a high value indicates that more information was available in the data to estimate that particular parameter, and that a more accurate parameter estimate could be obtained.

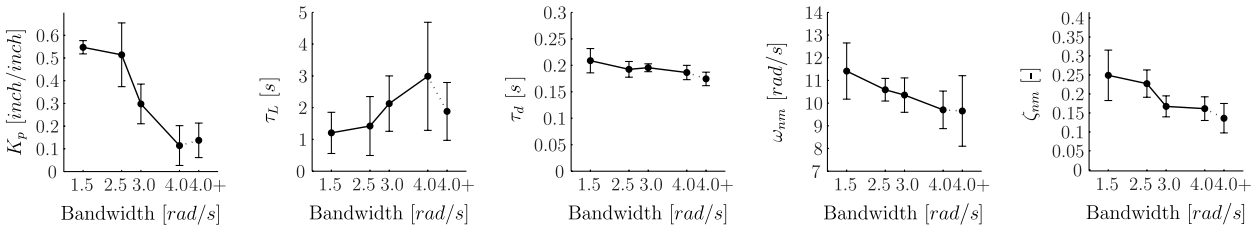

a) Operator gain **b) Lead time constant** **c) Pure time delay** **d) Neuromuscular bandwidth** **e) Neuromuscular damping**

Fig. 22 Means and 95% CI, corrected for between-subject variability.

Table 3 Results of repeated-measures ANOVA on PM parameters, where ∗∗ is highly significant ($p < 0.01$), ∗ is significant ($0.01 \leq p < 0.05$), and — is not significant ($p \geq 0.05$)

Independent variable	Dependent measures									
	K_p		τ_L		τ_d		ω_{nm}		ζ_{nm}	
	F(4, 16)	Sig.	F(4, 16)	Sig.	F(4, 16)	Sig.	F(3.28, 12.75)	Sig.	F(4, 16)	Sig.
Bandwidth	22.19	∗∗	2.427	—	3.078	∗	2.14[a]	—	5.689	∗∗

[a]Sphericity assumption not met, Greenhouse–Geisser [33] correction applied.

The figure illustrates that the accuracy in estimating the gain K_p remained approximately equal. The accuracy of the other parameters diluted in conditions 4 and 5 where participants regressed their crossover frequency. The estimates of pure time delay τ_d, neuromuscular frequency ω_{nm}, and neuromuscular damping ζ_{nm} all have lower normalized $\overline{\text{CRLB}}$ values. Generally speaking, these observations support hypothesis 2: the accuracy of the PM parameter estimates decreases when crossover regression occurs.

The accuracy of the lead time shows a different effect: for the 4.0 rad/s condition, the accuracy was severely degraded, whereas for the 4.0 + rad/s condition, the accuracy was approximately the same as for the 1.5 and 2.5 rad/s conditions. Note that this strengthens the observation that, in the 4.0+ condition, participants again adopted a relatively fixed strategy, as in the lower forcing-function bandwidth conditions, whereas apparently in condition 4.0 rad/s, there was still considerable variation in selecting the right strategy to cope with the high-frequency forcing-function components.

D. Hypothesis 3: Control-Behavior Linearity

The means and 95% confidence intervals of the relative remnant ρ_a^2 determined using both a nonparametric ARX fit and a parametric MLE fit are shown in Figs. 25a and 25b, respectively. Both methods show an increase between the 1.5 and 3.0 rad/s conditions and a marked decrease beyond this condition. For the 4.0 and 4.0+ conditions, the lowest values of the relative remnant were found. The effect for the MLE relative remnant was not significant; a significant effect was found for the ARX remnant (see Table 4).

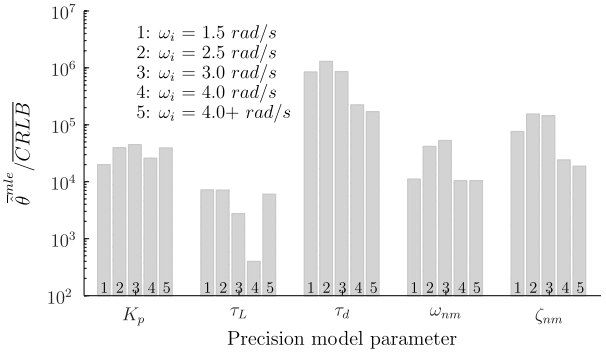

Fig. 24 Averaged values of the Cramér-Rao lower-bound normalized to the average parameter magnitude.

The means and 95% confidence intervals of the mean-squared remnant intensity $\bar{n}^2$, computed only for the MLE fit, are shown in Fig. 25c. On average, the remnant intensity was approximately the same for all conditions.

Individual values of the MS remnant intensity, group means, and standard deviations are shown in Fig. 26. Remnant was notably larger for participant 1 in comparison to the other participants. No clear trends regarding a potential adjustment of the remnant intensity for different forcing-function bandwidths can be found.

Figure 27 shows the linear correlation coefficients ρ^2 for participants 1, 4, and 5. At center frequencies, operators behaved almost linearly: $\rho^2 \approx 1$. At low frequencies, linearity degraded and a small amount of linearity was also lost at higher frequencies.

For all participants, the lowest linear correlations were found in the 4.0 and 4.0 + rad/s conditions. Combined with the relative remnant findings, this supports hypothesis 3: linearity in operator control behavior reduces when crossover regression occurs.

E. Hypothesis 4: Operator Time Delays

An overview of the three definitions of operator time delays (Sec. III.A) is given in Fig. 28. The ANOVA results, summarized in Table 5, indicate that the effects of the forcing-function bandwidth on the three time-delay definitions were all significant.

The PM pure delay (Fig. 28a) and the SPM effective time delay (Fig. 28b) both decrease proportionally with forcing-function bandwidth. The PM pure delay for the 4.0 + rad/s condition is approximately 30 ms lower than the delay for the 1.5 rad/s bandwidth. Recall that the difference between the SPM effective time delay and the PM pure time delay is caused by the neuromuscular contribution $\zeta_{\text{nm}}/\omega_{\text{nm}}$ [see Eq. (15)].

Figure 28c shows that the COM effective time delay decreases almost linearly in the 1.5, 2.5, and 3.0 rad/s conditions. It then increases sharply in the conditions where participants exhibited crossover regression, the 4.0 and 4.0 + rad/s bandwidth conditions. This supports hypothesis 4; the COM effective time delay increases after the occurrence of crossover regression. The increase originates from the equalization contribution [see Eq. (15)]. Note that the COM effective time-delay values deviate slightly but still compare very well to those reported by McRuer et al. [1].

F. Hypothesis 5: Closed-Loop Input-to-Error Spectrum

The closed-loop input-to-error spectra of participants 3 and 4, for all conditions, are shown in Fig. 29. A pronounced difference can be seen between the regressive conditions (4.0 and 4.0 + rad/s) and all other conditions. Here, the input-to-error peak decreases and

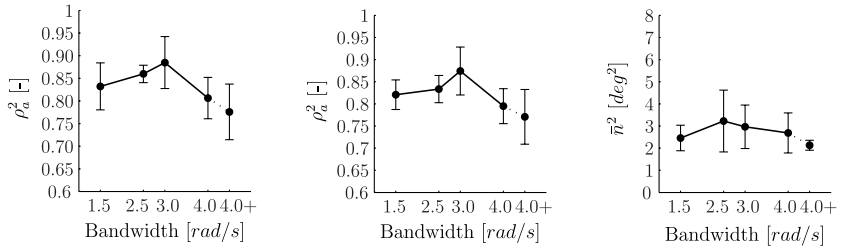

a) Relative remnant (ARX) **b) Relative remnant (MLE)** **c) Mean squared remant intensity (MLE)**

Fig. 25 Means and 95% CI, corrected for between-subject variability.

Table 4 Results of repeated-measures ANOVA on linearity and remnant metrics, where ∗ is significant ($0.01 \leq p < 0.05$) and — is not significant ($p \geq 0.05$)

Independent variable	Dependent measures					
	ρ_a^2 (MLE)		ρ_a^2 (ARX)		$\bar{n}^2$	
	F(1.3, 5.1)	Sig.	F(4, 16)	Sig.	F(4, 16)	Sig.
Bandwidth	3.326[a]	—	3.375	∗	0.99	—

[a]Sphericity assumption not met, Greenhouse–Geisser [33] correction applied.

stretches over a larger frequency range, a direct consequence of the reduction in operator gain. This decrease in maximum closed-loop input-to-error ratio is achieved at the cost, however, of a reduction in the low-frequency error suppression.

The maximum peak in input-to-error of participant 3 first increases (from the 1.5 rad/s to the 3.0 rad/s condition) and then suddenly becomes much smaller after he regressed his crossover frequency. Participant 4 shows a more gradual decrease of the maximum peak input-to-error, already from the 1.5 rad/s to the 3.0 rad/s conditions, followed by an also quite smooth reduction to the 4.0 rad/s and 4.0+ conditions. In the latter reduction, however, the low-frequency error suppression became much worse.

Figure 30 shows the maximum closed-loop input-to-error approximation $|e/i|^2_{\max}$. Between the 1.5 and 2.5 rad/s conditions, it slightly increases. Here, apparently, more effective error suppression at center frequencies is achieved by a *higher* maximum input-to-error amplification ratio (see Fig. 29a). Starting at the 3.0 rad/s condition, however, the maximum closed-loop input-to-error amplification ratio reduces significantly. This result supports hypothesis 5, which stated that the maximum closed-loop input-to-error ratio will decrease after the occurrence of crossover regression. After the decrease between the 2.5 and 4.0 rad/s conditions, the ratio of the 4.0 + rad/s condition is approximately the same as for the 4.0 rad/s condition. When considering the decrease in the COM effective time delay between the 1.5 and 3.0 rad/s conditions, the decrease in maximum input-to-error ratio beyond the 2.5 rad/s condition can only be attributed to a reduction in crossover frequency [recall Eq. (9)].

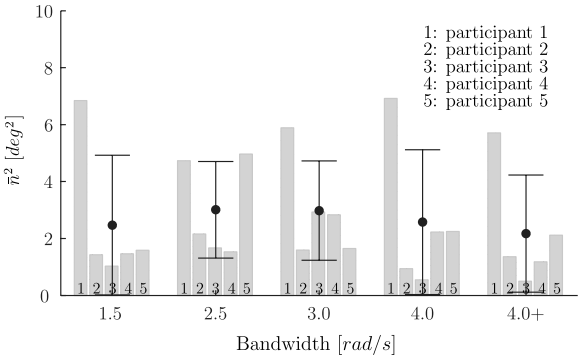

Fig. 26 Individual mean-squared remnant intensity.

VI. Discussion and Recommendations

In this section, we will discuss the theoretical and experimental results and provide recommendations for future work. We aim to answer the two main questions posed at the start of the paper. First, how do human operators adjust their settings (e.g., neuromuscular system, equalization), what is the between-subject variability, and what about the linearity of their control behavior when crossover regression occurs? Second, what is the general cause of crossover regression, and how can we better predict it?

A. Operator Control Behavior in Regressed Conditions

1. *Between-Subject Variability*

The frequency at which crossover regression occurs was found to depend on the participant. Generally speaking, two types of regression could be observed.

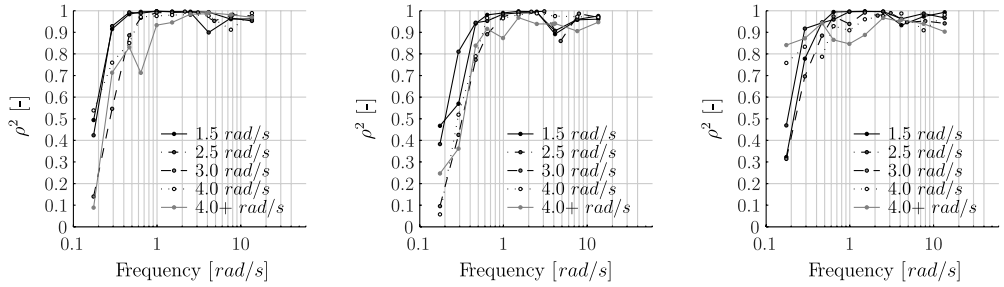

a) Participant 1 **b) Participant 4** **c) Participant 5**

Fig. 27 Squared correlation coefficient for three participants and all conditions.

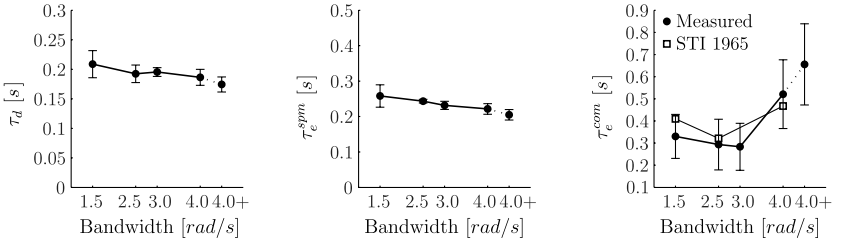

a) PM pure time delay **b) SPM effective time delay** **c) COM effective time delay**

Fig. 28 Means and 95% CI, corrected for between-subject variability.

Table 5 Results of repeated-measures ANOVA on human-operator time delays, where ∗ is significant ($0.01 \leq p < 0.05$)

Independent variable	Dependent measures					
	τ_e^{com}		τ_e^{spm}		τ_d (from Table 3)	
	F(1.42, 5.67)	Sig.	$\chi^2(4)$	Sig.	F(4, 16)	Sig.
Bandwidth	6.583[b]	∗	10.88[a]	∗	3.078	∗

[a]Normality assumption not met, Friedman's ANOVA used instead.
[b]Sphericity assumption not met, Greenhouse–Geisser [33] correction applied.

Three of our five participants reduced their crossover frequency considerably (two at the 3.0 rad/s condition, one at the 4.0 rad/s condition). These three participants showed very similar adaptation effects, increasing their lead-time constant from the 1.5 to 3.0 rad/s conditions, then a sudden decrease in lead and crossover frequency.

The two other participants tried to compensate for the forcing-function resonance in the 4.0 rad/s condition through a dramatic increase in their lead time. They regressed too, however, at the most difficult 4.0+ condition. Although their crossover frequencies and MS control activity were markedly higher, their NMSE performance was the same or only slightly better. Clearly, their investment in generating lead did not pay off very well.

As a result of the different strategies, the between-subject variation in crossover frequency increased considerably. Whereas for the regressive conditions, participants could be divided in two groups, these groups were not apparent in the nonregressive conditions.

The largest between-subject variations were found for the forcing functions that bring participants to the verge of crossover regression: the 3.0 and 4.0 rad/s conditions. In the conditions where either none of the participants (1.5 and 2.5 rad/s conditions) or all of the participants (the 4.0+ condition) regressed their crossover frequency, between-subject variability was relatively small.

The difficulties that occurred in the regression conditions were also reported by the participants. Overall, they commented that it was more difficult to find and, in particular, to hold on to a successful control strategy for the regressive conditions. After the completion of a typical 4.0 or 4.0 + rad/s run, participants often had no clue about their performance, whereas a fairly accurate judgment could be given in the other conditions.

2. *Parameter Adjustment*

The PM parameters, and especially the lead equalization and neuromuscular bandwidth, showed more variation in the regressive conditions. To reduce the maximum input-to-error magnitude, higher phase margins are beneficial. Then, in any operator attempt to generate more phase, the linear precision model parameters allow for a number of, possibly simultaneously occurring, adaptations [see Eq. (15)].

First, the pure time delay τ_d and neuromuscular damping ζ_{nm} can be decreased, which is indeed what we found in our experiment. Whereas McRuer et al. [1] assumed the pure time delay τ_d to be fixed, our results show a significant and almost proportional reduction (in total 30 ms) when forcing-function bandwidth increased. It is unclear whether this is an estimation artifact or an operator adjustment that is not yet understood.

Second, the neuromuscular frequency ω_{nm} could be increased; the opposite was found, however, in our data. It could well be that a simultaneous decrease of ζ_{nm} *and* increase in ω_{nm} is a difficult adaptation for the neuromuscular system. Perhaps the strategy of reducing the damping with a decrease of neuromuscular frequency, as found in this experiment, is somehow the best or easiest way to adapt the neuromuscular dynamics to reduce equivalent time-delay effects. This is mere speculation, however, and more research is needed to validate this hypothesis.

The contribution of the lead time to the effective COM time delay is small for large values of τ_L and large values of ω_c [Eq. (15)]. Hence, it is beneficial to have high lead values, and this is indeed what we found for the two participants that resisted crossover regression the most, participants 1 and 4. These participants show a large increase in their lead-time constant for the 4.0 rad/s condition, as compared to the lower-bandwidth conditions, in an attempt to decrease τ_e^{com}. Note that, even when there is no lead (not possible for double integrator dynamics), it would still be worthwhile to have a crossover frequency that is as high as possible.

3. *Comparison to the 1965 STI Experiment*

For the nonregressive 1.5 and 2.5 rad/s conditions, our results correspond very well to those reported in McRuer et al. [1]. Our participants exhibited higher crossover frequencies, but similar performance in the 1.5 and 2.5 rad/s conditions. This is in line with the theoretical mean-squared error analysis: higher crossover frequencies do not necessarily result in better performance. In fact, the NSME was found to correspond much better with phase margin, whereas crossover frequency was a better predictor of MS control activity. For the 4.0 rad/s condition, our participants had more difficulty in suppressing the NMSE as compared to the STI participants.

4. *Linearity in Operator Control Behavior*

Overall, higher levels of nonlinear effects and corresponding remnant levels in operator control behavior were observed in the

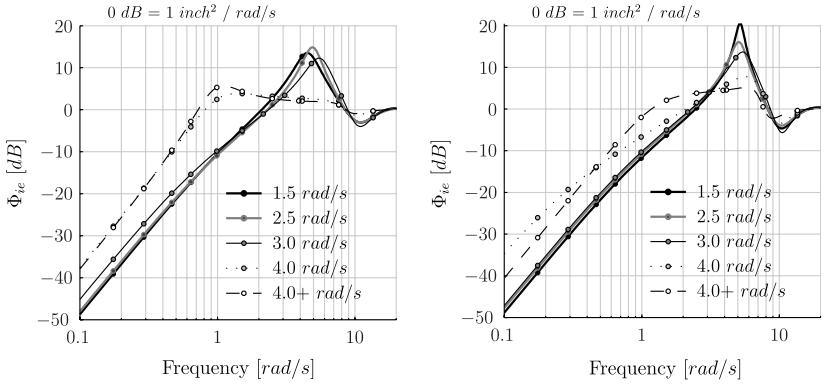

a) Participant 3 **b) Participant 4**

Fig. 29 Closed-loop input-to-error spectra.

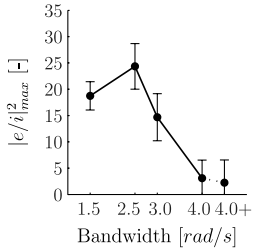

Fig. 30 Means and 95% CI, corrected for between-subject variability, of maximum input-to-error ratio.

regressed conditions. As a consequence, the accuracy in the nonparametric ARX fit and in the PM parameter estimates decreased.

The goodness of fit, described by the relative remnant, for both ARX and MLE methods shows a marked decrease for the regressive 4.0 and 4.0 + rad/s conditions. The correlation coefficient ρ^2 was lowest for these conditions, also at the center frequencies, whereas in the other conditions, the operator behaved almost linearly in this important frequency region. The Cramér-Rao results indicate that, whereas the pure time delay could be estimated quite accurately, the operator lead time was the most difficult parameter to estimate, especially in the 4.0 rad/s condition.

Note that, generally speaking, the degraded accuracy of the estimated parameters for the regressive 4.0 and 4.0 + rad/s conditions might be explained by the nature of crossover regression. Here, the operator ignores large parts of the forcing function, in particular the high-frequency content; therefore, less information regarding operator control behavior is available in the data at these high-frequencies, resulting in poor signal-to-noise ratios and deteriorating parameter estimation accuracy. Clearly, the frequency-domain identification techniques used in this investigation have problems in coping with these conditions; other techniques might yield better results.

B. Causes of Crossover Regression and Prediction of the Phenomenon

1. *Causes*

The increase in closed-loop damping between the 3.0 and 4.0 rad/s conditions exemplifies the principle of crossover regression: participants achieved better error suppression by "slowing-down the system response," a strategy to reduce the closed-loop forcing-function resonance at center frequencies, that is, the frequencies near the crossover region.

The experiment results clearly show that, with larger forcing-function bandwidths, participants try to reduce their time delay, which is always advantageous from the perspective of lowering the maximum input-to-error ratio [Eq. (9)]. But then, first at the 3.0 rad/s condition (for three participants), and also at the 4.0 rad/s condition (for the other two participants), the time-delay reduction was insufficient. The excessive forcing-function resonance at center frequencies could then only be reduced by decreasing the crossover frequency, which in turn led to a marked increase in the COM effective time delay [see Eq. (15) and Fig. 28].

2. *Prediction*

In our experiment, similar to the 1965 STI experiment, crossover regression occurs for the higher-bandwidth forcing-function conditions. As has been discussed extensively in Sec. III, reducing the operator's effective time delay is always advantageous, whereas a reduction in crossover frequency depends on the placement (in particular, high) frequencies of the forcing function. In this respect, an analysis of the variation in NMSE as a function of crossover frequency, yielding a figure like Fig. 5, can provide an early insight into whether crossover regression may or may not occur.

In our experiment, operator control behavior considerably changed in the 4.0+ condition as compared to the 4.0 rad/s condition. Note that these two forcing functions had the same bandwidth and also the same signal power. Apparently, positioning another sinusoid component in the range of the center frequencies, while keeping bandwidth and signal power the same, forces operators to adapt their control behavior considerably. Their NMSE got worse, MS control activity (and rate) decreased, crossover frequency and phase margin reduced; closed-loop stability remained more or less the same.

Regarding the PM parameters, the pure time delay, neuromuscular damping, and, in particular, the lead-time constant decreased considerably, whereas pilot gain increased. Additionally, behavior became more nonlinear, as for this condition the lowest relative remnant and linear correlations were found for *lower* values of the remnant power.

Clearly, more efforts are needed to investigate the effects of forcing-function definitions on operator behavior, and results of a first investigation have been promising [34].

C. Recommendations

Based on the preceding analyses, the following recommendations are made.

First, in our experiment, the conditions were randomized in blocks and participants had to adjust their control strategy between runs. Repeating each condition a number of times within each block could have resulted in better and perhaps also a less variable adjustment of the control strategy in the conditions where crossover regression occurred.

Second, it is clear that crossover regression should be avoided when one intends to use linear models and keep the variability in human control behavior within bounds. Our experiment showed that human control behavior becomes much more variable, and different strategies to cope with the forcing-function resonance start to emerge. Hence, to reduce the already infamous diversity in human adaptation to experimental task variables, it is recommended to use forcing functions that have reasonably low bandwidths, where McRuer's inequality [$\omega_i < 0.8\omega_c$, Eq. (2)] holds.

Third, it is shown that linear identification methods are unable to capture the nonlinear effects associated with crossover regression. To enhance identification in experiments that aim at triggering crossover regression, we should investigate how the linear precision model can be extended to capture the regressive control behavior or whether nonlinear operator models are needed.

Also, the use of identification methods that can better capture nonlinearities in human behavior should be better investigated. In this respect, the time-domain MLE methods show the largest potential [22].

Finally, our findings call for more extensive research into the role of forcing-function characteristics on operator control behavior. Apparently, the two parameters that are often assumed to be paramount in the selection of good forcing functions, bandwidth and signal power, are not sufficient in completely characterizing (and safeguarding) the possible effects of the forcing function on human performance and control behavior.

VII. Conclusions

A theoretical and experimental investigation was conducted to obtain a better understanding of the crossover regression phenomenon. It was found that a generalized cause of crossover regression is the human constraint in reducing the crossover model effective time delay. The resulting excessive forcing-function resonance around the crossover frequency causes closed-loop tracking performance to deteriorate rapidly and forces the operator to regress his crossover frequency. The bandwidth of the forcing function where crossover regression occurs was found to depend on the participant, however, and between-subject variability increased considerably in regressed conditions.

Linear-operator model parameters were more variable in these conditions, especially the lead-time constant and neuromuscular frequency. Additionally, human control behavior was found to be more nonlinear. Linear models could only capture a part of the observed behavior and the accuracy of the parameter estimates deteriorated.

We recommend that, in the design of manual tracking experiments, when linear models are intended to be used, the experimenter should prevent crossover regression. In addition, we recommend that, in the actual design of manual controls, the occurrence of crossover regression should be prevented, because the overall performance in regressive conditions is significantly lower than in nonregressive conditions. This imposes requirements on both the tracking signal, as well as on the control element dynamics.

More research is needed to investigate the effects of forcing-function characteristics, other than bandwidth and signal power, on human tracking behavior and performance.

References

[1] McRuer, D. T., Graham, D., Krendel, E. S., and Reisener, W., Jr., "Human Pilot Dynamics in Compensatory Systems. Theory, Models, and Experiments with Controlled Element and Forcing Function Variations," U.S. Air Force Flight Dynamics Lab., TR AFFDL-TR-65-15, Wright–Patterson AFB, OH, 1965.

[2] Hess, R. A., "Effects of Time Delays on Systems Subject to Manual Control," *Journal of Guidance, Control, and Dynamics*, Vol. 7, No. 4, 1984, pp. 416–421. doi:10.2514/3.19872

[3] Groot, T., Damveld, H. J., Mulder, M., and Van Paassen, M. M., "Effects of Aeroelasticity on the Pilot's Psychomotor Behavior," AIAA Paper 2006-6494, Aug. 2006.

[4] Damveld, H. J., "A Cybernetic Approach to Assess the Longitudinal Handling Qualities of Aeroelastic Aircraft, Ph.D. Thesis, Faculty of Aerospace Engineering, Delft Univ. of Technology, Delft, The Netherlands, 2009.

[5] Johnston, D. E., and Aponso, B. L., "Design Considerations of Manipulator and Feel System Characteristics in Roll Tracking," Systems Technology, NASA-CR 4111, 1988.

[6] Hess, R. A., "Modeling the Effects of Display Quality upon Human Pilot Dynamics and Perceived Vehicle Handling Qualities," *IEEE Transactions on Systems, Man, and Cybernetics*, Vol. 25, No. 2, 1995, pp. 338–344. doi:10.1109/21.364831

[7] McRuer, D. T., and Krendel, E. S., "Mathematical Models of Human Pilot Behavior," Systems Technology TR STI-P-146, 1974.

[8] Hosman, R. J. A. W., "Pilot's Perception and Control of Aircraft Motions," Ph.D. Thesis, Faculty of Aerospace Engineering, Delft Univ. of Technology, Delft, The Netherlands, Nov. 1996.

[9] Van der Vaart, J. C., "Modelling of Perception and Action in Compensatory Manual Control Tasks," Ph.D. Thesis, Faculty of Aerospace Engineering, Delft Univ. of Technology, Delft, The Netherlands, Dec. 1992.

[10] Pool, D. M., Mulder, M., Van Paassen, M. M., and Van der Vaart, J. C., "Effects of Peripheral Visual and Physical Motion Cues in Roll-Axis Tracking Tasks," *Journal of Guidance, Control, and Dynamics*, Vol. 31, No. 6, 2008, pp. 1608–1622. doi:10.2514/1.36334

[11] Elkind, J. I., "Characteristics of Simple Manual Control Systems," Ph.D. Thesis, Lincoln Lab., Massachusetts Inst. of Technology, Cambridge, MA, 1956.

[12] Gordon-Smith, M., "An Investigation Into Certain Aspects of the Describing Function of a Human Operator Controlling a System of One Degree of Freedom," Univ. of Toronto, Inst. of Aerospace Studies, TR UTIAS 149, Toronto, Ontario, Canada, Feb. 1970.

[13] McRuer, D. T., and Jex, H. R., "A Review of Quasi-Linear Pilot Models," *IEEE Transactions on Human Factors in Electronics*, Vol. HFE-8, No. 3, 1967, pp. 231–249. doi:10.1109/THFE.1967.234304

[14] Jex, H. R., and Magdaleno, R. E., "Corroborative Data on Normalization of Human Operator Remnant," *IEEE Transactions on Man-Machine Systems*, Vol. 10, No. 4, 1969, pp. 137–140. doi:10.1109/TMMS.1969.299912

[15] Kleinman, D. L., Baron, S., and Levison, W. H., "An Optimal Control Model of Human Response, Part I: Theory and Validation," *Automatica*, Vol. 6, No. 3, 1970, pp. 357–369. doi:10.1016/0005-1098(70)90051-8

[16] Kleinman, D. L., Baron, S., and Levison, W. H., "An Optimal Control Model of Human Response, Part II: Prediction of Human Performance in a Complex Task," *Automatica*, Vol. 6, No. 3, 1970, pp. 371–383. doi:10.1016/0005-1098(70)90052-X

[17] de Jong, J. N. M., and van Lunteren, A., "Human Operator Remnant in a Subcritical Task," *Proceedings of the Eighth Annual Conference on Manual Control*, NASA, Washington, D.C., May 1972, pp. 565–588.

[18] Kleinman, D. L., and Baron, S., "Manned-Vehicle Systems Analysis by Means of Modern Control Theory," NASA NASA-CR 1753, 1971.

[19] Dehouck, T. L., Mulder, M., and Van Paassen, M. M., "Effects of Simulator Motion Filter Settings on Pilot Control Behavior," AIAA Paper 2006-6250, Aug. 2006.

[20] Duppen, M., Zaal, P. M. T., Mulder, M., and Van Paassen, M. M., "Effects of Motion on Pilot Behavior in Target, Disturbance and Combined Tracking Tasks," AIAA Paper 2007-6894, Aug. 2007.

[21] Praamstra, F. J., Pool, D. M., Zaal, P. M. T., Ellerbroek, J., Mulder, M., and Van Paassen, M. M., "Function of State Perception in Human Control Behavior in Target Tracking Tasks," AIAA Paper 2008-6845, Aug. 2008.

[22] Zaal, P. M. T., Pool, D. M., De Bruin, J., Mulder, M., and Van Paassen, M. M., "Use of Pitch and Heave Motion Cues in a Pitch Control Task," *Journal of Guidance, Control, and Dynamics*, Vol. 32, No. 2, 2009, pp. 366–377. doi:10.2514/1.39953

[23] Van Paassen, M. M., and Mulder, M., "Identification of Human Control Behavior," *International Encyclopedia of Ergonomics and Human Factors*, 2nd ed., edited by W. Karwowski, Taylor and Francis, London, 2006, pp. 400–407, ISBN 041530430X.

[24] Mulder, M., and Mulder, J. A., "A Cybernetic Analysis of Perspective Flight-Path Display Dimensions," *Journal of Guidance, Control, and Dynamics*, Vol. 28, No. 3, 2005, pp. 398–411. doi:10.2514/1.6646

[25] Nieuwenhuizen, F. M., Zaal, P. M. T., Mulder, M., Van Paassen, M. M., and Mulder, J. A., "Modeling Human Multi-Channel Perception and Control Using Linear Time-Invariant Models," *Journal of Guidance, Control, and Dynamics*, Vol. 31, No. 4, 2008, pp. 999–1013. doi:10.2514/1.32307

[26] Söderström, T., and Stoica, P., *System Identification*, Prentice–Hall, Cambridge, England, U.K., 1989, pp. 149–151.

[27] Ljung, L., *System Identification: Theory for the User*, 2nd ed., Prentice–Hall, Upper Saddle River, NJ, 1999, pp. 69–81, chap. 4.

[28] Zaal, P. M. T., Mulder, M., Van Paassen, M. M., and Mulder, J. A., "Maximum Likelihood Estimation of Multi-Modal Pilot Control Behavior in a Target-Following Task," *Proceedings of the IEEE Conference on Systems, Man, & Cybernetics (IEEE—SMC), Singapore*, Inst. of Electrical and Electronics Engineers, New York, Oct. 2008, pp. 1085–1090.

[29] Zaal, P. M. T., Pool, D. M., Chu, Q. P., Van Paassen, M. M., Mulder, M., and Mulder, J. A., "Modeling Human Multimodal Perception and Control Using Genetic Maximum Likelihood Estimation," *Journal of Guidance, Control, and Dynamics*, Vol. 32, No. 4, 2009, pp. 1089–1099. doi:10.2514/1.42843

[30] Lunney, G. H., "Using Analysis of Variance with a Dichotomous Dependent Variable: an Empirical Study," *Journal of Educational Measurements*, Vol. 7, No. 4, 1970, pp. 263–269.

[31] Lindquist, E. F., "*The Design and Analysis of Experiments in Psychology and Education*," Houghton Mifflin, Boston, 1953.

[32] Wasicko, R. J., McRuer, D. T., and Magdaleno, R. E., "Human Pilot Dynamics Response in Single-Loop Systems with Compensatory and Pursuit Displays," Systems Technology TR AFFDL-TR-66-137, 1966.

[33] Greenhouse, S. W., and Geisser, S., "On Methods in the Analysis of Profile Data," *Psychometrika*, Vol. 24, No. 2, June 1959, pp. 95–112. doi:10.1007/BF02289823

[34] Beerens, G. C., Damveld, H. J., Mulder, M., Van Paassen, M. M., and Van der Vaart, J. C., "Design of Forcing Functions for Identification of Human Control Behavior," AIAA Paper 2009-6026, Aug. 2009.